© 2016. Published by The Company of Biologists Ltd | Journal of Cell Science (2016) 129, 2586-2598 doi:10.1242/jcs.186585

RESEARCH ARTICLE

VEGF-A stimulates podosome-mediated collagen-IV proteolysis in microvascular endothelial cells

Thomas Daubon[1,*,§], Pirjo Spuul[1,2,‡,§], Florian Alonso[1,2], Isabelle Fremaux[1,2] and Elisabeth Génot[1,2,¶]

ABSTRACT

Podosomes are dynamic cell–matrix contact structures that combine several key abilities, including adhesion, matrix degradation and mechanosensing. These actin-based cytoskeletal structures have been mostly studied in monocytic cells, but much less is known about those formed in other lineages. In this study, we characterise podosomes in capillary-derived microvascular endothelial cells. We identify two types of podosomes: constitutive podosomes that form in the absence of specific stimulation and induced podosomes that arise in response to the angiogenic factor VEGF-A. Constitutive and VEGF-A-induced podosomes share similar components but exhibit marked differences in terms of gelatinolytic activity. We also show that the extracellular matrix proteins laminin and collagen-IV are key determinants of the VEGF-A response, but neither collagen-I nor fibronectin are conducive for podosome induction. Moreover, only collagen-IV elicits the formation of proteolytically active podosomes through a mechanism involving increased Src phosphorylation, p190RhoGAP-B (also known as ARHGAP5) relocalisation and MT1-MMP (also known as MMP14) cell surface exposure at podosome sites. We hypothesise that by promoting podosome formation, VEGF-A enables endothelial cells to overcome the basement membrane barrier to allow sprouting outwards from the existing vasculature.

KEY WORDS: Podosomes, Endothelial cells, VEGF-A, Collagen-IV, Basement membrane

INTRODUCTION

Vascular endothelial cells line the entire circulatory system from the heart to the smallest capillaries and play a key role in the maintenance and remodelling of the vascular system. The physiology of these cells depends heavily on cytoskeleton rearrangements that are controlled by soluble factors, matrix proteins, cell–cell interactions and mechanical forces. Actin-based cytoskeletal structures called podosomes have been described in endothelial cells (Billottet et al., 2008) and the elucidation of their precise role in endothelial biology thus represents a major challenge. So far, most of our knowledge on podosomes comes from studies performed in macrophages, osteoclasts or immature dendritic cells where they are most commonly found. They are described as dynamic cell–matrix contact structures that combine several key abilities, including adhesion, matrix degradation and mechanosensing (Linder and Kopp, 2005; Linder and Wiesner, 2015). Although the triggering signal for podosome initiation is not known yet, Src family kinases have a pivotal role in their formation (Murphy and Courtneidge, 2011). Structurally, podosomes comprise a core of F-actin associated with actin regulatory proteins such as Arp2/3, WASp or N-WASp (also known as WAS and WASL, respectively), cortactin, dynamin, gelsolin and cofilin, which contribute to their dynamic behaviour, and the scaffolding protein and Src substrate Tks5 (also known as SH3PXD2A), which constitutes a reliable podosome marker. Around the central core, integrins, adaptors and signalling proteins, including FAK (also known as PTK2), vinculin, talin and paxillin, form an adhesive ring domain. Recent studies have shown that acto-myosin filaments radiating from the dense F-actin cores interconnect podosomes and enable their collective behaviour (Proag et al., 2015; van den Dries et al., 2013).

In contrast to cells of the myelomonocytic lineage, where podosomes develop evenly in the first steps of integrin-mediated cell spreading, podosome formation is an inducible phenomenon for endothelial cells. Most studies have been performed with human umbilical vein endothelial cells (HUVECs) (Osiak et al., 2005) exposed to phorbol esters (Guegan et al., 2008; Seano et al., 2014; Tatin et al., 2006) or with aortic endothelial cells exposed to TGFβ (Curado et al., 2014; Varon et al., 2006). In these situations, podosomes arise in clusters or ring-shaped superstructures that are often called rosettes. However, recent studies have shown that matrix proteins are also involved in podosome induction, architecture and arrangement. In the absence of any specific cytokine (or pharmacological) stimulation, a collagen-I (Col-I) substrate elicits the formation of atypical linear podosomes aligning along collagen fibrils (Juin et al., 2013), whereas in a confined environment, fibronectin induces the formation of either isolated entities or podosome rosettes (Spuul et al., 2015). Such diversity points to a multiplicity of regulatory mechanisms for podosome formation in endothelial cells and raises the question of whether these podosomes are functionally equivalent.

Podosome-forming cells share the common feature of traveling across tissues, suggesting that podosome lytic enzymes overcome extracellular matrix (ECM) barriers. Among them, the transmembrane matrix metalloprotease MT1-MMP (also known as MMP14) is found at podosomes in all types of cells forming these structures and plays a prominent role (Linder, 2007). However, *in vitro*, many studies are limited to the use of the traditional fluorescent gelatin invasion assay that highlights the matrix-degrading capabilities of podosomes, showing only the gelatinolytic activity on the denatured Col-I matrix. Thus, it remains unclear whether podosomes are used by cells to travel across all types of ECM encountered during their transtissular migration or if there are cell type and matrix protein specificities for their induction and function.

[1]Université de Bordeaux, 33 000 Bordeaux, France. [2]INSERM U1045, 33 000 Bordeaux, France.
*Present address: Department of Biomedecine, University of Bergen, Postboks 7804, Bergen N-5009, Norway. ‡Present address: Department of Gene Technology, Tallinn University of Technology, Akadeemia Rd 15, Tallinn 12618, Estonia.
§These authors contributed equally to this work

¶Author for correspondence (elisabeth.genot@inserm.fr)

T.D., 0000-0003-0622-7946; P.S., 0000-0001-9410-721X; F.A., 0000-0002-6794-1513; I.F., 0000-0002-3632-6016

Received 21 January 2016; Accepted 19 May 2016

Journal of Cell Science

Journal of Cell Science (2016) 129, 2586-2598 doi:10.1242/jcs.186585

In the context of angiogenesis, degradation of the ECM scaffold enables the vasculature to be reshaped (Davis and Senger, 2005). Endothelial cells within existing blood vessels breach the basement membrane [whose main components are collagen-IV (Col-IV) and laminin], which forms a sleeve around the capillary, to escape from the parent vessel and migrate within the interstitial matrix (mainly composed of Col-I and fibronectin), which is found between cells. Neovessel formation is completely abroagated in MT1-MMP-null mice (Chun et al., 2004). To explore the role of podosomes during the angiogenesis invasive step, we chose to use microvascular cells (human microvascular endothelial cells, HMVECs), which form the sprouting capillaries, and examine their response to the canonical angiogenic factor VEGF-A. We also used various matrices to address their substrate specificities and characterised podosome proteolytic capacities under each condition. We found that a small fraction of the HMVEC population assembled podosomes upon adhesion regardless of the matrix. When cells were exposed to VEGF-A, podosome formation was stimulated but this response occurred only on basement membrane proteins. Finally, we found that Col-IV, but not laminin, stimulated the formation of matrix-degrading podosomes upon VEGF-A stimulation. Collectively, these results show that podosomes display cell type and matrix protein specificities for their induction and function.

RESULTS

HMVECs spontaneously assemble podosomes and VEGF-A stimulates their formation

We used primary HMVECs for these studies as physiological angiogenesis involves endothelial cells from capillaries. HMVECs are large cells with prominent stress fibres (Fig. 1A). At the lowest confocal plan, we found F-actin colocalised with cortactin, Tks5 and other podosomal proteins (Linder and Aepfelbacher, 2003) (Fig. S1) in punctate structures forming circular clusters or rings. These were identified as genuine podosome rosettes by performing the gelatin degradation assay (Fig. 1B) and by the detection of MT1-MMP and phosphorylated Src (active Src) (Tatin et al., 2006; Varon et al., 2006) markers (Fig. 1C). We also visualised the typical polygonal arrangement of vinculin around F-actin and cortactin cores (Walde et al., 2014), and F-actin interconnecting cables by stimulated emission depletion (STED) microscopy (Labernadie et al., 2010; Luxenburg et al., 2007; van den Dries et al., 2013) (Fig. 1D). In these unstimulated cultures, the proportion of podosome-forming cells never exceeded 5.5% of the total cell population.

We next examined whether the number of cells presenting podosome rosettes was altered upon angiogenic stimulation. In HUVECs, VEGF stimulates podosome formation with a peak response observed 5 min after the addition of the cytokine and a return to baseline values 1 h later (Osiak et al., 2005). A prompt dose-dependent increase in podosome-forming cells also occurred in HMVECs exposed to soluble VEGF-A, but this response (20 min) reached its maximum at 24 h (Fig. 1E–G). In the gelatin assay, matrix degradation became detectable after 1 h and steadily increased for the first 3 h (Fig. 1H–J). However, after that point, the degradation index of VEGF-A-treated cells increased dramatically and both the number and size, as well as the intensity of degraded areas (loss of matrix fluorescence) rose significantly (Fig. 1K,L). The pattern of the degraded areas in the fluorescent matrix suggested several possibilities in terms of cell motility: a reduced motility of VEGF-treated cells that would stay still and degrade larger holes in the matrix before crawling away, an increased motility of these cells, leaving behind more numerous holes over a wide area, or a combination of both. We therefore first analysed cells individually, then classified them into two groups, matrix-degrading and non-degrading cells, that we followed over a period of three consecutive hours in the second phase of the 24-h response to VEGF-A (i.e. at least 3 h after adhesion onset, Fig. 1H,I). Regarding matrix-degrading cells, we found that VEGF-A-treated cells had a higher velocity and higher displacement as compared to untreated cells. For non-degrading cells, velocity and displacement were not significantly different between the two groups (Fig. S2). We conclude that the matrix degradation pattern observed for VEGF-treated cells results from both a higher degradation potential (Fig. 1L) and a multiplication of degradation areas associated with their higher motility.

Because VEGF-A stimulates cell proliferation in sparse cultures, podosome induction could be somehow linked to the mitotic state. We therefore compared podosome formation and matrix degradation in sparse and confluent cultures. In addition, this exploration had the potential to provide some insights into the *in vivo* situation where endothelial cells form a continuous lining in the microvessel. By itself, confluence favoured podosome rosette formation but this response was insensitive to VEGF-neutralising antibodies, thus ruling out an autocrine effect (Fig. 2A,B). Collectively, these results indicate that VEGF-A is a regulator of podosome formation and function for HMVECs. We distinguished two classes of podosomes, constitutive podosomes with low degrading capacities whose formation was stimulated shortly after VEGF-A addition, and induced podosomes that had acquired a higher degrading potential upon prolonged VEGF-A exposure.

As none of the tested markers (Fig. S1) discriminated between the two types of podosome rosettes, we examined the cell subpopulations. The sialomucin CD34 is a surface adhesion glyocoprotein that has been shown to be expressed in a small subset of cultured endothelial cells (Siemerink et al., 2012). No direct correlation could be established between these cells and podosome-forming cells (Fig. 2C). However, confluence failed to stimulate podosome formation in either untreated or VEGF-A-treated CD34-positive cells (Fig. 2C), suggesting that this signal was already part of their phenotype. In unstimulated cultures, CD34-positive cells were morphologically similar to CD34-negative cells (Fig. 2D). In contrast, VEGF-A-stimulated CD34-positive cells were polarised and presented filopodia (Fig. 2D).

VEGF-A-induced podosomes differ qualitatively from constitutive podosomes

MT1-MMP and MMP2 localise at podosomes in HUVECs (Guegan et al., 2008; Osiak et al., 2005; Tatin et al., 2006). Besides its important contribution to ECM cleavage, MT1-MMP also acts as a membrane-anchored activator, processing inactive pro-MMP2 into active MMP2 at the cell surface. We therefore analysed the expression, localisation and activity of MT1-MMP after 24 h of VEGF-A stimulation in HMVECs. VEGF-A treatment did not alter MT1-MMP expression levels in cells seeded on either uncoated or gelatin-coated substrata (Fig. 3A,B). As MT1-MMP is known to be actively transported to the cell surface of podosome sites (Wiesner et al., 2010), we also examined MT1-MMP cell surface exposure in control and stimulated cells seeded on gelatin. The analysis of biotinylated cell surface proteins revealed greater exposure of MT1-MMP at the surface of VEGF-A-stimulated HMVECs than in untreated cells (Fig. 3C). Again, similar results were obtained when cells were seeded on uncoated substrata (Fig. 3D). MT1-MMP staining of non-permeabilised cells was brighter at podosome rosettes in VEGF-A-treated cells than in controls (Fig. 3E–G).

Journal of Cell Science (2016) 129, 2586-2598 doi:10.1242/jcs.186585

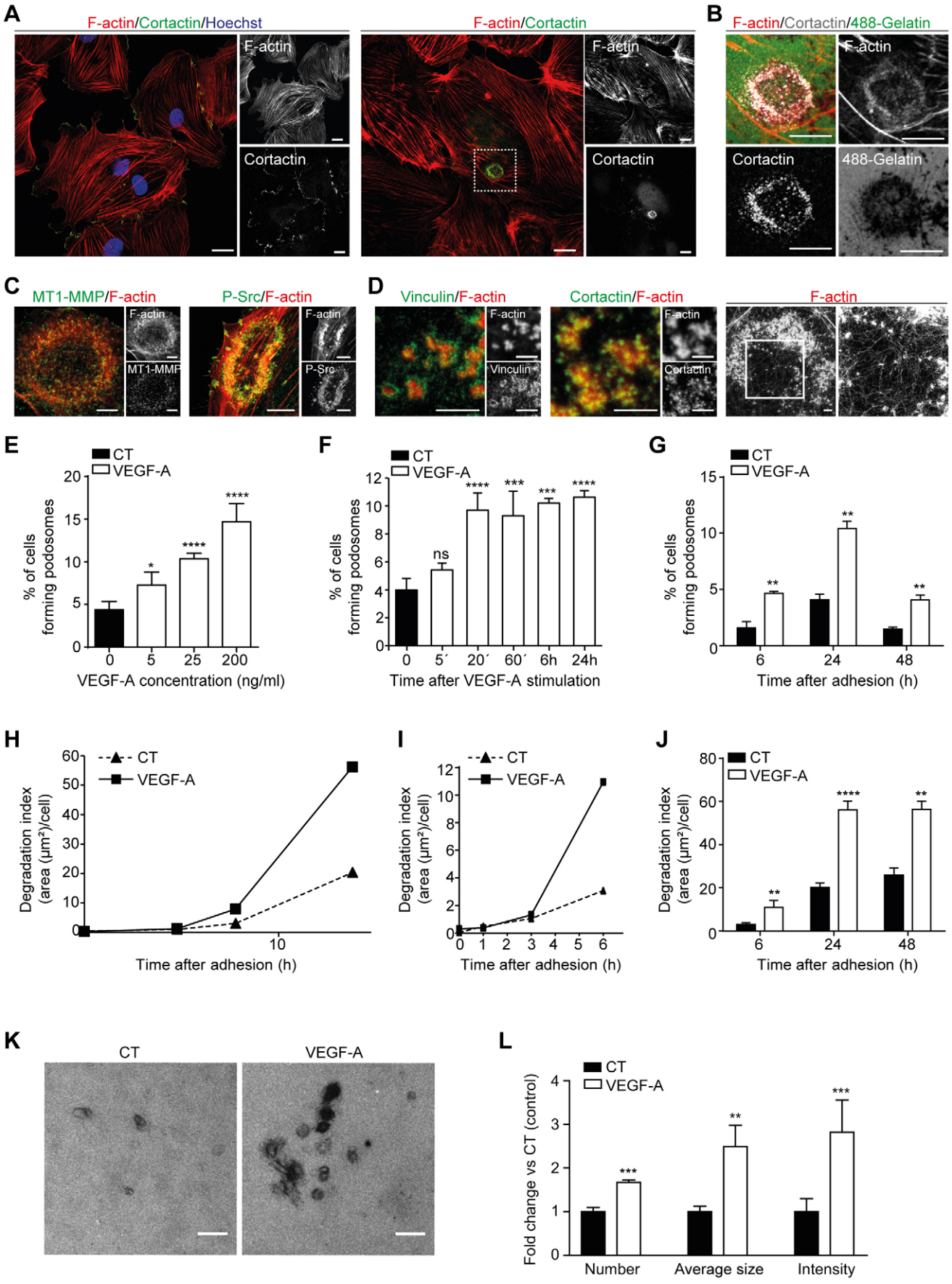

Fig. 1. See next page for legend.

Journal of Cell Science (2016) 129, 2586-2598 doi:10.1242/jcs.186585

Fig. 1. HMVECs spontaneously assemble podosome rosettes that mature upon VEGF-A stimulation. (A) Representative image of HMVECs triple-stained for F-actin, cortactin and nuclei (left panel) and of one cell (right panel) showing a podosome rosette (boxed region) at the level of the plasma membrane. Single stainings for F-actin and cortactin are shown in the side panels. Scale bars: 20 µm. (B) The podosome rosette shown in the boxed region in A and the underlying Oregon-Green-488-conjugated gelatin matrix underneath; the individual stainings show localised matrix degradation at the podosome rosette. Scale bars: 10 µm. (C) Podosome markers and F-actin at podosome rosettes. Scale bars: 5 µm. (D) Stimulated emission depletion (STED) super-resolution images of podosome rosettes showing the typical string arrangement of vinculin (confocal image for F-actin), revealing patchy staining for cortactin (confocal image for F-actin), and in the last panel, the interconnecting F-actin cables between individual podosomes within the rosette. Scale bars: 2 µm. (E) Graph showing the podosome response (F-actin and cortactin) as a function of VEGF-A concentration after 20 min of stimulation. CT, control (no stimulation). (F) Timecourse of the VEGF-A (25 ng/ml) response for cells seeded on glass coverslips and (G) the maximum response 24 h after cell adhesion onto gelatin. (H) Graph showing a marked increase in the degradation index (degraded area per cell) after cell adhesion onto gelatin and (I) detail of the time window where the shift occurs. (J) The degradation index corresponding to the podosome response (such as shown in G) shows the activity plateauing 24 h after cell adhesion onto the gelatin. In E–G, n=3 individual experiments in which 300 cells were analysed per experimental point, mean±s.d. is shown. *P<0.05; **P<0.01; ***P<0.001; ****P<0.0001; ns, not significant (one-way ANOVA Bonferroni multiple comparison test compared with respective CT). For H,I, one representative experiment is shown. In J, n=3 independent experiments in which 10 fields (1500 cells) were analysed per experimental point, mean±s.d. is shown. **P<0.01, ****P<0.0001 (one-way ANOVA Bonferroni multiple comparison test compared with respective CT). (K) Representative images of the gelatin coating illustrating the increased matrix degradation upon 24 h of VEGF-A stimulation. Scale bars: 50 µm. (L) Graph showing the increase in the number (per 1 mm^2), size and intensity (loss of matrix fluorescence) of degraded areas in 24 h-VEGF-A-treated cells versus controls. n=3 independent experiments in which degraded areas from 10 fields were analysed per experimental point, mean±s.d. is shown, **P<0.01, ***P<0.001 (Student's t-test compared with respective CT).

Taken together, these results indicate that VEGF-A-induces a qualitative change in podosome rosettes over a 24-h period and that increased MT1-MMP cell surface exposure discriminates between VEGF-A-induced podosomes and constitutively formed podosomes.

MT1-MMP regulation depends on multiple intracellular trafficking events (Linder and Wiesner, 2015). In HUVECs, p190RhoGAP-B (also known as ARHGAP5) regulates MT1-MMP cell surface presentation (Guegan et al., 2008) but its regulation by VEGF-A has not been explored. We observed more recruitment of p190RhoGAP-B to VEGF-A-induced podosomes than constitutive podosomes in HMVECs, but no change for p190RhoGAP-A (also known as ARHGAP35) or ARAP3, a third RhoGAP component (Guegan et al., 2008; Yu et al., 2013) (Fig. 4A). The cellular expression levels of the three proteins remained unaltered upon VEGF-A stimulation (Fig. 4B). Silencing p190RhoGAP-B had no effect on constitutive podosomes but it selectively suppressed the VEGF-A-induced podosome rosettes and associated gelatinolytic capacities (Fig. 4C–E). These results indicate that p190RhoGAP-B could also be involved in podosome induction. To get some insights into how p190RhoGAP-B regulates the podosome increase in response to VEGF-A, we focused our analysis on its function. Because p190RhoGAP-B exhibits its catalytic activity preferentially towards RhoA, we evaluated RhoA activity at podosomes using a conformation-specific monoclonal antibody that recognises RhoA-GTP but not RhoA-GDP. VEGF-A stimulation was associated with an increase of RhoA-GTP at podosomes and depletion of p190RhoGAP-B prevented this response (Fig. 4F). Taken together, these data indicate that podosome induction in response to VEGF-A stimulation is associated with increased MT1-MMP exposure at podosome sites through a pathway involving p190RhoGAP-B, which contributes to the spatial regulation of RhoA activity at podosomes.

VEGF-A regulates podosome formation only on basement membrane proteins and proteolyses Col-IV selectively

We next examined the contribution of genuine ECM proteins to VEGF-A-induced podosome formation. *In vitro*, HMVECs produced Col-IV, laminin, Col-I and fibronectin, and VEGF-A stimulated the expression of Col-IV (Fig. 5A). When cells were seeded on these proteins, a small fraction of the HMVEC population assembled podosomes upon adhesion regardless of the matrix (Fig. S3). We observed both the short-term and long-term VEGF-A podosome responses on the basement membrane proteins Col-IV, laminin and Matrigel (a mixture of ECM components containing predominantly laminin and to a lesser extent Col-IV), but no induction on fibronectin or Col-I (Fig. 5B). Accordingly, matrix degradation was stimulated on Col-IV but not on fibronectin or Col-I (Fig. 5C–E). As expected, Col-I also elicited the formation of collagenolytic linear podosomes along fibrils (Juin et al., 2012) but VEGF-A did not increase the number of cells presenting them (Fig. 5F,G). In agreement with previous findings in an *ex vivo* set-up (Rottiers et al., 2009), HMVEC podosome rosettes were unable to degrade laminin. Laminin–FITC remained a suitable substrate for other types of podosomes, such as those formed by MDA-MB-231 cells (Fig. S4A). Thus, Col-IV was found to be the only matrix protein that stimulates basement membrane degradation upon treatment of cells with VEGF-A.

We then verified MT1-MMP exposure at podosome sites upon VEGF-A stimulation in cells plated on Col-IV versus laminin substrata. On Col-IV, a quantitative analysis of MT1-MMP cell surface exposure showed that MT1-MMP staining of non-permeabilised cells was consistently more intense with VEGF-A-treated cells than with untreated cells. In contrast, no differences were found when cells were seeded on laminin or Matrigel (Fig. 5H,I), indicating that MT1-MMP was not recruited to podosome rosettes elicited on these matrices. Podosome rosettes stained for α2β1 integrin in cells seeded on Col-IV but α6β1 integrin was absent from the podosome areas when cells were seeded on laminin (Fig. S4B).

Collectively, these results indicate that basement membrane proteins are conducive for podosome formation in HMVECs exposed to VEGF-A and that podosomes mediate Col-IV but not laminin degradation. In contrast, VEGF-A does not promote podosome formation in HMVECs seeded on either fibronectin or Col-I.

Basement-membrane-dependent responses to VEGF-A regulate podosome formation and function

Given that p190RhoGAP-B expression appeared to be essential for podosome induction, we examined its relocalisation upon VEGF-A stimulation when cells were seeded on the various ECM proteins. Increased recruitment of p190RhoGAP-B at podosomes was observed only when cells were seeded on Col-IV matrices (Fig. 6A). Because laminin did not elicit such a response, p190RhoGAP-B relocalisation did not appear to be the signalling component for podosome induction on this matrix protein but rather for the podosome-degrading function. We also explored Src regulation as Src both interacts with adhesion molecules and is a

Journal of Cell Science (2016) 129, 2586-2598 doi:10.1242/jcs.186585

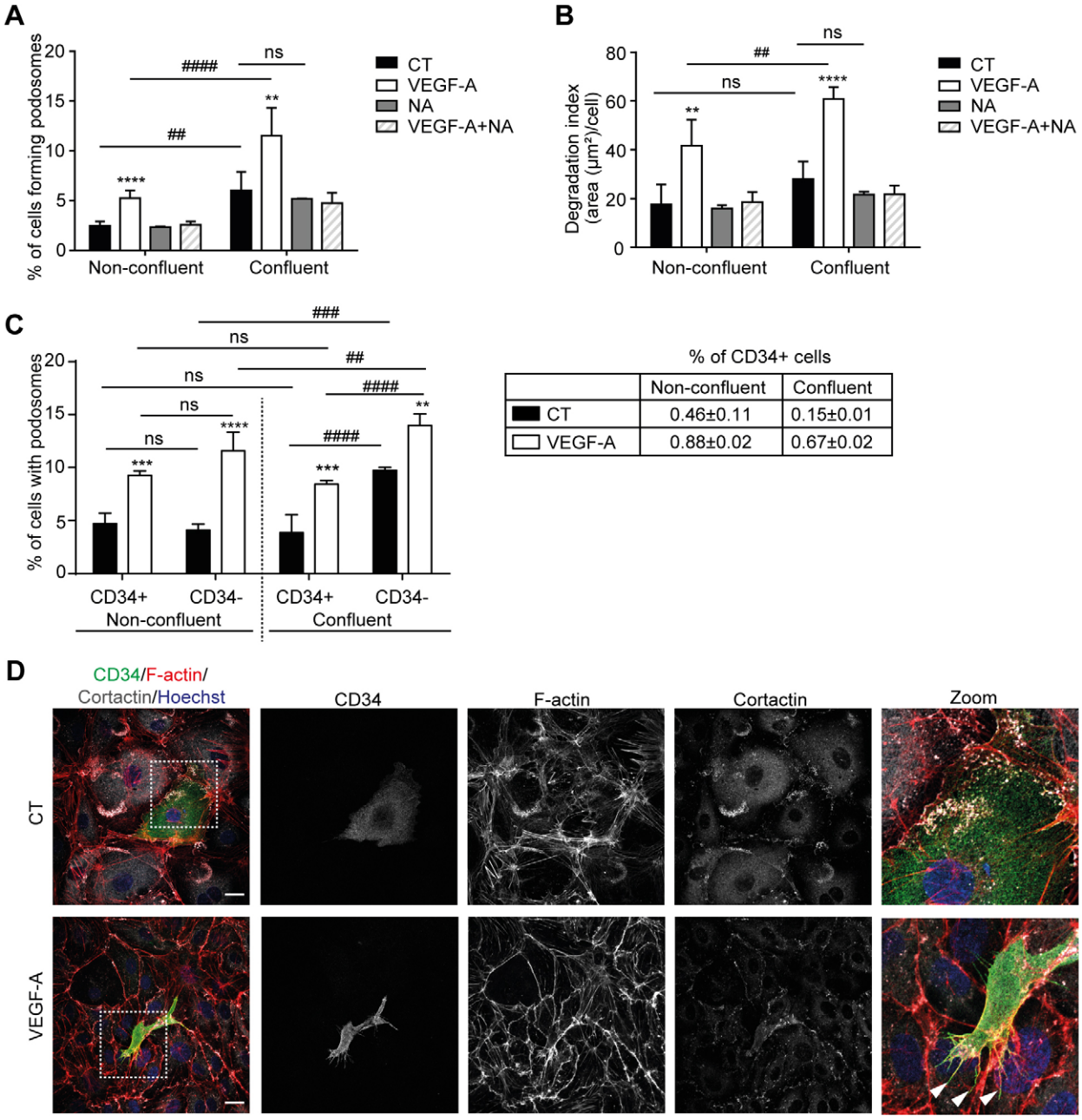

Fig. 2. Cell confluence also affects podosome formation. (A) Graph showing the percentage of cells forming podosome rosettes (F-actin and cortactin staining) in either sparse or confluent HMVEC cultures, in the presence or absence of VEGF-A neutralising antibodies (NA). CT, control (no stimulation). (B) Matrix degradation index corresponding to the podosome response shown in A. Note that confluence stimulates podosome formation in a VEGF-A-independent manner. (C) Graph showing the percentage of cells forming podosome rosettes (F-actin and cortactin staining) in $CD34^-$ and $CD34^+$ subpopulations in either sparse or confluent HMVEC cultures. Note that cell confluence stimulates podosome formation and associated matrix degradation only in the CD34- subpopulation. *n*=3 individual experiments in which 300 cells (for podosome formation) or 10 fields (for degradation) were analysed per experimental point, mean±s.d. is shown. $^{**,\#\#}P<0.01$; $^{****,\#\#\#\#}P<0.0001$; $^{***,\#\#\#}P<0.001$; ns, not significant (one-way ANOVA Bonferroni multiple comparison test was used compared with respective CT or as indicated). (D) Representative images showing the morphology of $CD34^+$ cells in HMVEC cultures analysed in C. Podosome rosettes were found in both $CD34^-$ and $CD34^+$ cells. Note filopodia extending from elongated polarised VEGF-A-treated $CD34^+$ HMVECs (arrowheads) but not in adjacent $CD34^-$ HMVECs with cobblestone morphology (bottom panel). Nuclei were stained with Hoechst 33342 (blue). Scale bars: 20 µm.

crucial downstream effector of VEGF receptors (Claesson-Welsh and Welsh, 2013). By analysing the autophosphorylation of Tyr418 within the kinase activation loop as a marker of Src activation, we found that Col-IV, but none of the other matrices, enhanced Src activity in HMVECs exposed to VEGF-A (Fig. 6B). Combined, these results show that Col-IV synergises with VEGF-A to regulate podosome induction and degrading function.

DISCUSSION

Most of our knowledge on podosomes comes from studies performed in cells of the monocytic lineage, that is, single cells which form these cytoskeletal structures spontaneously. However, podosomes have now been described in many other cell types where they have the fundamental difference of being inducible but not constitutive. Podosome architecture and arrangement also

Journal of Cell Science (2016) 129, 2586-2598 doi:10.1242/jcs.186585

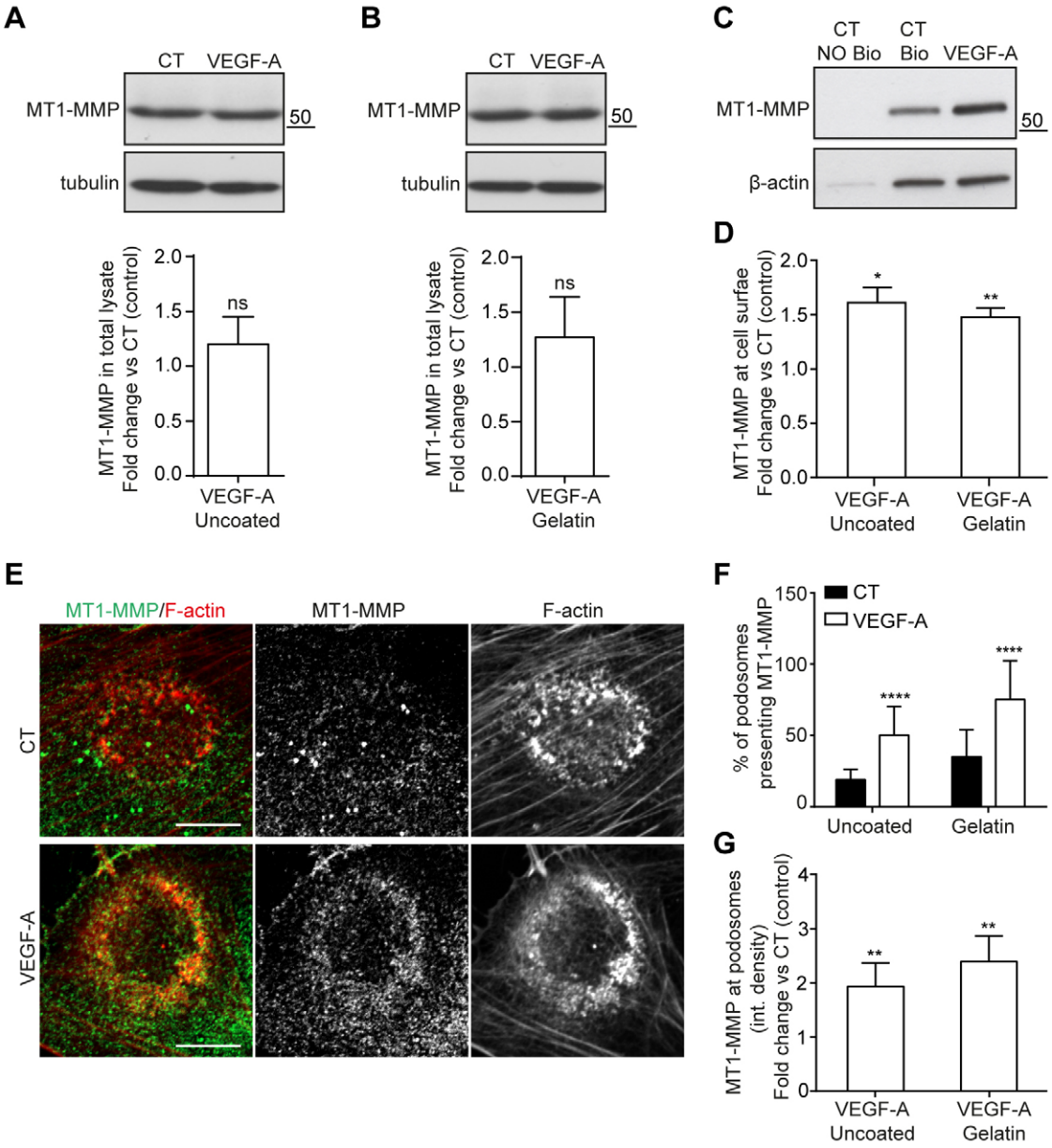

Fig. 3. VEGF-A stimulates MT1-MMP exposure at the cell surface. Analysis of MT1-MMP expression in protein extracts from control (CT) and VEGF-A-treated HMVECs seeded on uncoated (A) or gelatin-coated (B) culture dishes. The quantification shown in the graph below indicates the mean±s.d. fold change in MT1-MMP expression normalised to tubulin in HMVECs seeded on uncoated or gelatin-coated dishes from three independent experiments. (C) Biotinylated cell-surface proteins (Bio) and non-biotinylated (NO Bio) intracellular proteins were affinity-purified on streptavidin beads from control and VEGF-A-treated HMVECs seeded on gelatin, then analysed by immunoblotting using anti-MT1-MMP and anti-β-actin antibodies, respectively. (D) Quantification of MTI-MMP at the cell surface in the conditions shown in C and in conditions where cells were seeded on uncoated dishes from three independent experiments. Data is shown as mean±s.d. fold change compare to CT Bio and normalised to β-actin. For A, B and D, **P*<0.05, ***P*<0.01; ns, not significant (Student's *t*-test). (E) Representative images showing differential MT1-MMP staining at podosome rosettes in non-permeabilised untreated and VEGF-A-stimulated HMVECs seeded on gelatin-coated coverslips, counterstained with phalloidin after permeabilisation. Scale bars: 10 µm. (F,G) Statistical analysis of the number of podosomes presenting MTI-MMP (F) and MT1-MMP staining at podosomes (G) in the conditions shown in E and in conditions where cells were seeded on uncoated coverslips. *n*=3 independent experiments in which 10 rosettes per experimental point were analysed, mean±s.d. is shown. In G, data is shown as fold change compare to CT. ***P*<0.01, *****P*<0.0001 (Student's *t*-test).

vary depending on the cell type being considered (Juin et al., 2012, 2013; Spuul et al., 2015). This raises the question as to what extent our knowledge on monocytic cell podosomes can be extrapolated to those found in other cell lineages. In this study, we characterised podosomes formed by microvascular endothelial cells, which form the capillary endothelium *in vivo*. We identified two types of podosomes, constitutive podosomes that form in adherent endothelial cells in the absence of specific stimulation and induced podosomes that arise in response to VEGF-A. In both situations, endothelial cell podosomes were organised in rosettes and the basic bipartite podosome architecture remained similar to that described for individual podosomes in monocytic cells. In endothelial cells, we also visualised the actin cables interconnecting neighbouring podosomes, which are probably instrumental in generating the characteristic rosette pattern.

Journal of Cell Science (2016) 129, 2586-2598 doi:10.1242/jcs.186585

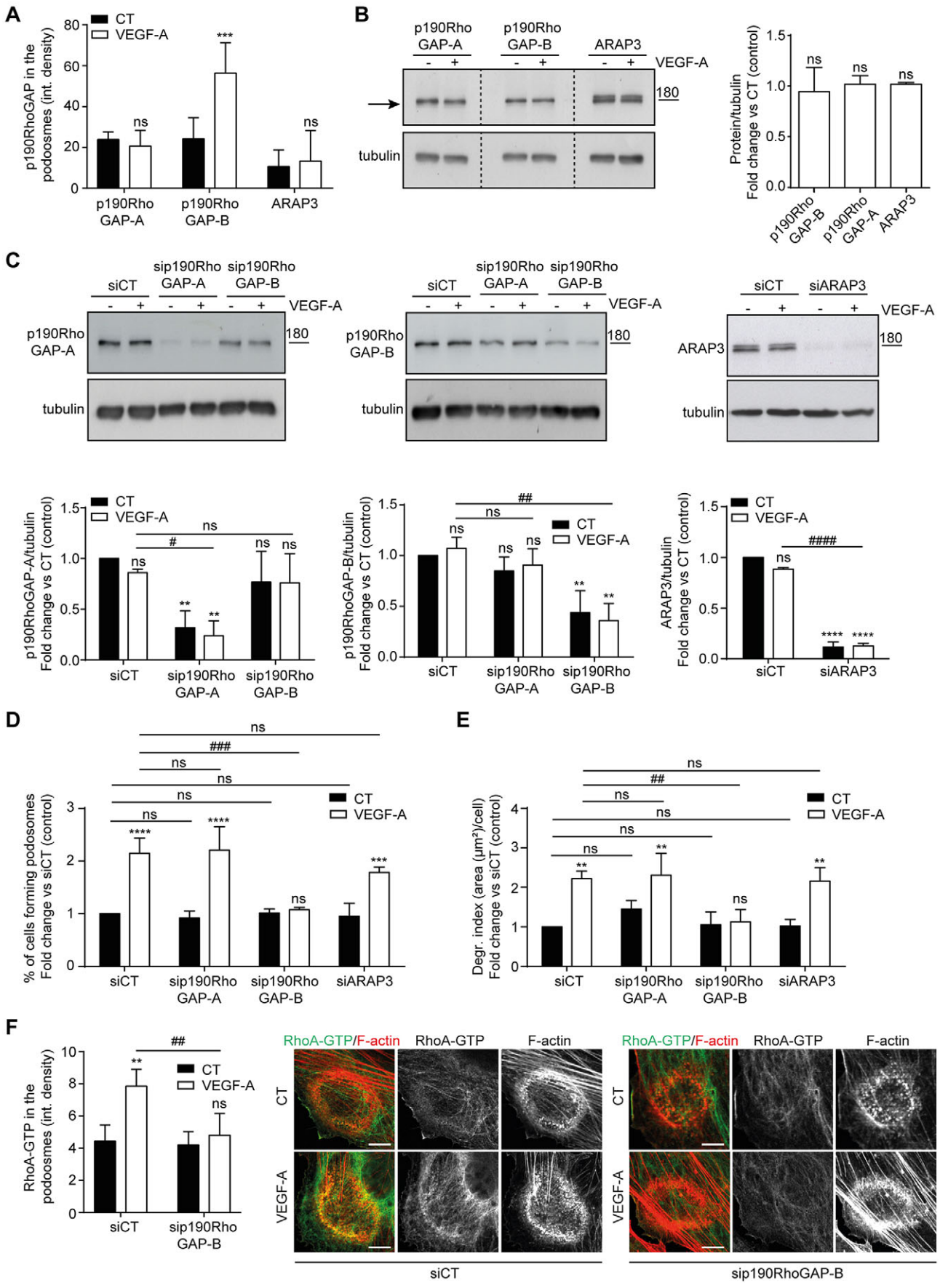

Fig. 4. See next page for legend.

Journal of Cell Science (2016) 129, 2586-2598 doi:10.1242/jcs.186585

Fig. 4. p190RhoGAP-B depletion inhibits VEGF-A-induced podosomes and associated matrix degradation. (A) Quantitative analysis of p190RhoGAP localisation at podosomes presented as integrated density (defined as the product of area and mean grey value) showing increased recruitment of p190RhoGAP-B at podosomes in VEGF-A-stimulated cells; *n*=3 independent experiments in which 10 rosettes per experimental point were analysed, mean±s.d. is shown. CT, control (no stimulation). ***P<0.001; ns, not significant (Student's *t*-test compared with CT). (B) Analysis of p190RhoGAP-A, p190RhoGAP-B and ARAP3 expression (arrow) in protein extracts from control and VEGF-A-treated HMVECs seeded on uncoated culture dishes. The quantification shown in the graph indicates the mean±s.d. fold increase in their expression normalised to tubulin in each condition from three independent experiments. ns, not significant (Student's *t*-test). (C) Immunoblots of protein extracts from HMVECs transfected with control (siCT), p190RhoGAP-A (sip190RhoGAP-A), p190RhoGAP-B (sip190RhoGAP-B) or ARAP3 (siARAP3) siRNA, untreated or treated with VEGF-A, and blotted for either p190RhoGAP-A, p190RhoGAP-B or ARAP3. Knockdown efficiency is shown in the quantification below for the protein expression levels normalised to tubulin in each condition (mean±s.d. of three independent experiments). $^{\#}P$<0.05; $^{**,\#\#}P$<0.01; $^{****,\#\#\#\#}P$<0. 0001; ns, not significant (one-way ANOVA Bonferroni multiple comparison test compared with siCT). (D) Quantitative analysis of the induction of podosome rosettes formed upon VEGF-A stimulation in p190RhoGAP-A-, p190RhoGAP-B- or ARAP3-depleted HMVECs seeded on Oregon-Green-488-conjugated gelatin-coated coverslips. (E) Corresponding degradation index in the experimental conditions shown in D. In D and E, *n*=3 individual experiments in which 300 cells (for podosome formation) or 10 fields (for degradation) were analysed per experimental point, mean±s.d. is shown. $^{**,\#\#}P$<0.01, $^{***,\#\#\#}P$<0.001; $^{****}P$<0.0001 (one-way ANOVA with Bonferroni multiple comparison test compared with respective CT or as indicated). (F) Quantitative analysis of RhoA-GTP localisation at podosomes in control and p190RhoGAP-B-depleted cells presented as integrated density. RhoA-GTP recruitment to podosomes is increased in VEGF-A-stimulated cells but p190RhoGAP-B depletion prevents it; *n*=3 independent experiments in which 10 rosettes per experimental point were analysed, mean±s.d. is shown. $^{**,\#\#}P$<0.01 (Student's *t*-test compared with respective CT). The right panels show representative images of RhoA-GTP (green) localisation at podosomes in conditions shown in the graph on the left. Podosome rosettes were counterstained with phalloidin (red). Scale bars: 10 µm.

In HMVECs, podosome formation appeared not to be restricted to the $CD34^{+}$ subpopulation (Siemerink et al., 2012). Rather, we found that confluence positively regulated podosome formation independently of VEGF-A, suggesting that either some junctional components or cell–cell communication and signalling pathways participate in this response. A link between junctional proteins and podosomes has been made because the actin-binding zonula occludens protein 1 (ZO-1) has been found at podosomes in smooth muscle cells (Kremerskothen et al., 2010). However, the involvement of Notch signalling, which links the fate decisions of one cell to those of its neighbours during angiogenesis, appear a more likely mechanism (Phng and Gerhardt, 2009). Here, we show that restoring cell–cell junctions and direct cell communication *in vitro* promotes podosome formation in a context where endothelial cells are activated by the *in vitro* culture conditions. Therefore, the relevance of these findings needs to be addressed *in vivo* using established angiogenesis models (Norrby, 2006).

We previously characterised the occurrence of podosomes in endothelial cells derived from liver sinusoids (LSECs) (Juin et al., 2013). These specialised capillaries exhibit morphological features that differentiate them from classical capillaries, such as the lack of a continuous basal membrane (Le Bail et al., 1990), which facilitates their specific functions in the liver. A large fraction of LSECs (>60%) in culture form constitutive podosomes and they do not organise in rosettes. In addition, VEGF-A does not detectably affect podosome formation in these cells. Thus, the constitutive podosomes in LSECs differ substantially from those found in HMVECs.

The podosome response to VEGF-A reached its maximum after 24 h, in contrast to HUVECs where the peak was observed at 5 min and the level returned to baseline within 1 h (Osiak et al., 2005). VEGF-A-induced and constitutive podosomes shared similar components but exhibited marked differences in terms of gelatinolytic activity. Such changes correlated with increased MT1-MMP cell surface exposure and increased recruitment of p190RhoGAP-B at podosomes. In addition, p190RhoGAP-B was also required for podosome induction in response to VEGF-A, suggesting that induced podosomes are assembled *de novo*. Although it is possible that p190RhoGAP-B regulates these two events independently, at this stage, we cannot exclude that MT1-MMP regulation impacts on podosome induction in response to VEGF-A. p190RhoGAP-B is known to be primarily regulated by subcellular localisation (Matheson et al., 2006) and to regulate the spatial regulation of RhoA activity (Ponik et al., 2013). In VEGF-A-stimulated HMVECs, we show that the local activation of RhoA at podosomes was dependent on p190RhoGAP-B. Thus, whereas constitutive podosomes are primarily regulated by cell confluence, VEGF-A-induced podosomes are controlled by a pathway involving p190RhoGAP-B.

As for cells of the myelomonocytic lineage, most substrata seem to be permissive to the formation of podosomes in HMVECs. However, some ECM proteins were found to be more favourable than others. Vitronectin is the preferential matrix for podosome formation in osteoclasts (Fuller et al., 2010) whereas fibrinogen is the best for macrophages (Labernadie et al., 2010). We have now found that laminin and Col-IV are the preferential substrates for podosome induction in HMVECs. These results contrast with those obtained with HUVECs, where laminin was shown to impair podosome formation (Seano et al., 2014). Our findings show the instrumental roles played by matrix proteins in podosome formation in various cell types and again highlight fundamental differences between endothelial cells originating from different vascular beds.

Our results also reveal a role for matrix proteins in the response to VEGF-A, which eventually dictate podosome function. In cells seeded on Col-IV, VEGF-A induced the formation of podosomes capable of degrading the underlying matrix, whereas, in cells seeded on laminin, VEGF-A induced inactive podosomes proteolytically. VEGF-A activates Src and this can occur through several pathways (Caron et al., 2009; Meyer et al., 2008; Sun et al., 2012). On Col-IV, VEGF-A stimulation increased Src autophosphorylation, p190RhoGAP-B relocalisation and MT1-MMP cell surface exposure at podosome sites whereas these events did not occur on laminin, thus suggesting differences in VEGF-A signalling on these two matrices. The molecular mechanisms of these responses remain to be established but likely involve signalling crosstalk between VEGF-A receptor and integrins (Plow et al., 2014).

The data presented in Table 1 summarise our findings. The results obtained on uncoated matrix were similar to those obtained on Col-IV, consistent with our finding that cultured HMVECs produce large amounts of Col-IV. Gelatin (denatured Col-I) gave similar results to those with globular Col-IV. Thus, in HMVECs, Col-IV is both a master regulator of podosome formation and a potent inducer of Col-IV degradation. We conclude that VEGF-A-induced podosomes in HMVECs subsume specific functions in relation to the basal membrane. They disrupt the Col-IV bonds to loosen the laminin–Col-IV scaffold (Rowe and Weiss, 2008), which subsequently leads to the dissociation of the laminin meshwork (Yurchenco et al., 2004). In these cells, laminin-induced podosomes

Journal of Cell Science (2016) 129, 2586-2598 doi:10.1242/jcs.186585

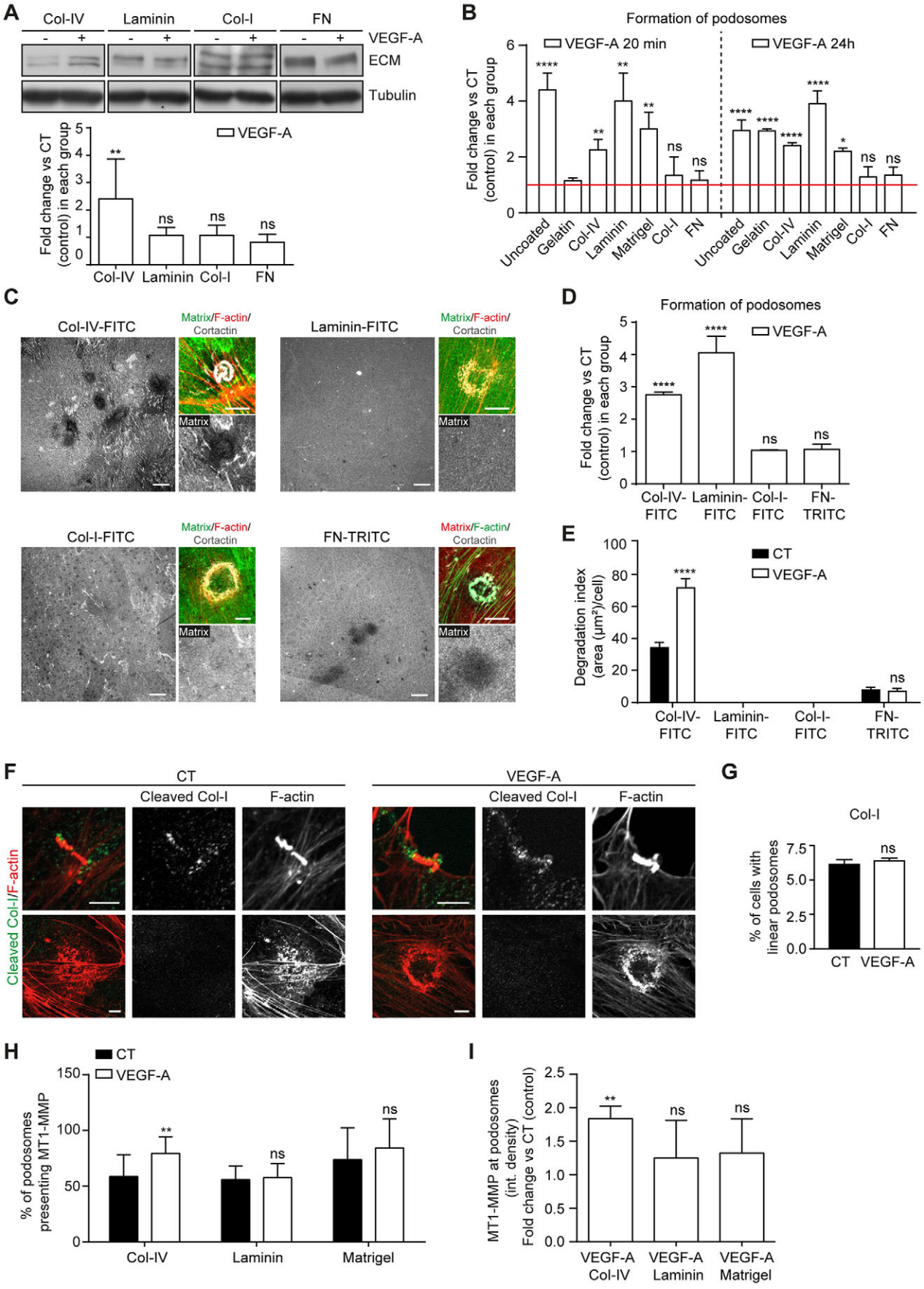

Fig. 5. See next page for legend.

Journal of Cell Science (2016) 129, 2586-2598 doi:10.1242/jcs.186585

Fig. 5. Matrix-dependent podosome specificities: VEGF-A favours podosome formation on basement membrane proteins and stimulates Col-IV degradation. (A) Western blots showing the ECM components (FN, fibronectin) produced by HMVECs *in vitro* over a 24-h stimulation period in the absence or presence of VEGF-A (25 ng/ml). Analysis of matrix protein expression in protein extracts from control and VEGF-A-treated HMVECs seeded on uncoated culture dishes. The quantification shown in the graph below indicates the mean±s.d. fold increase in their expression normalised to tubulin in each condition from five independent experiments. ns, not significant (one-way ANOVA Bonferroni multiple comparison test). (B) Graph showing podosome formation (F-actin and cortactin staining) in HMVECs seeded on various ECM proteins compared with uncoated substrata or gelatin (0.1%), upon a short (20 min) or long (24 h) exposure to VEGF-A. The mean±s.d. fold change compared with the control (CT) in each group is shown. (C) Representative images showing the degraded matrix at 24 h when fluorescent matrix proteins were used as substrata. Scale bars: 20 µm. The side panels show a podosome rosette (merge image of F-actin, cortactin and matrix in top panel) and the underlying matrix (single staining, bottom panel). Scale bars: 10 µm. (D) Quantitative analysis of the induction of podosome rosettes in HMVECs formed upon VEGF-A stimulation and (E) corresponding degradation index in the experimental conditions shown in C. The stimulatory effect of VEGF-A on podosome formation was observed when cells were seeded on basement membrane proteins and not on interstitial components. In B,D and E, n=3 individual experiments in which 300 cells (B,D) or 10 fields (E) were analysed per experimental point, mean±s.d. is shown. *P<0.05; **P<0.01; ****P<0.0001; ns, not significant (one-way ANOVA Bonferroni multiple comparison test). (F) Representative image of the F-actin structures (red) formed on Col-I-coated substrata and of their collagenolytic activity visualised by positive staining with antibody against the Col-I cleavage site (green) in untreated and VEGF-A-stimulated HMVECs (top panel). The bottom panel shows no Col-I degradation by podosome rosettes in these cells. Scale bars: 5 µm. (G) Quantification of linear podosomes in untreated and stimulated HMVECs showing no variation due to the VEGF-A exposure; n=3 independent experiments in which 300 cells per experimental point were analysed, mean±s.d. is shown. ns, not significant (Student's t-test). (H,I) Statistical analysis of the number of podosomes presenting MTI-MMP (H) and MT1-MMP staining at podosomes (I) in the experimental conditions shown in Fig. 3C, but with cells seeded on Col-IV, laminin or Matrigel; n=3 independent experiments in which 10 rosettes per experimental point were analysed, mean±s.d. is shown. In I, data is shown as fold change compare to CT. **P<0.01; ns, not significant (Student's t-test).

might mediate other podosomal function such as cell adhesion (Veillat et al., 2015). Interstitial matrix proteins did not promote podosome formation even in the presence of VEGF-A, suggesting that, during sprouting angiogenesis, podosomes are not involved in the migration that follows the extrication of the activated endothelial cell from the parental vessel (Davis and Senger, 2005). We hypothesise that by promoting podosome formation, VEGF-A enables endothelial cells to overcome the basement membrane barrier to allow sprouting from the existing vasculature as well as for re-entering the network by facilitating anastomosis of vessel segments cleared of basement membrane coverage.

MATERIALS AND METHODS

Cells, cell culture and cell stimulation

Human pulmonary microvascular endothelial cells (HMVECs, Lonza, tested free of contamination) were maintained in complete endothelial cell growth medium (EGM-MV; Promocell, a culture medium that does not contain VEGF) containing antibiotics at 37°C in a 5% CO_2 humidified atmosphere and used between passages two and seven. Cells were trypsinised and seeded in complete medium at 1×10^5 cells per plate in 3.5-cm dishes for western blot experiments or at 1.5×10^4 cells per glass coverslip in four-well plates for immunofluorescence imaging. For stimulation, human recombinant VEGF-A (used at 25 ng/ml in all experiments, except for the dose-response experiment) was obtained from Promocell. Neutralising VEGF antibodies (MAB293) were obtained from R&D Systems. Podosome formation assays were performed by double staining for F-actin and cortactin.

ECM protein coatings and ECM gels

Matrix protein coatings were performed on glass coverslips as follows: gelatin (Sigma), diluted to 0.1% in PBS at 37°C for 30 min; plasma-derived fibronectin (Sigma), diluted to 20 µg/ml in PBS at 37°C for 90 min; Matrigel (growth factor-reduced Matrigel™ basement membrane matrix, BD Biosciences) diluted with complete medium to 1 mg/ml at 37°C for 30 min; Col-IV (Sigma) diluted to 10 µg/ml in PBS at 4°C overnight; Col-I (Sigma), diluted to 0.2 mg/ml in PBS at 37°C for 30 min; and laminin (placental laminin containing mainly vascular LN-511, Sigma) diluted to 20 µg/ml in PBS at room temperature for 60 min. After washing with PBS, coverslips were incubated for at least 20 min with culture medium before adding the cells.

In situ matrix degradation assay

For the gelatin degradation assay, glass coverslips were first coated with Oregon-Green-488-conjugated gelatin diluted to 0.1% in PBS at room temperature for 30 min, washed with PBS and fixed with 0.5% glutaraldehyde (EMS) for 15 min. After washing with PBS, coverslips were incubated in 5 mg/ml sodium borohydride for 15 min under constant agitation, sterilised in 70% ethanol, then washed three times in PBS and finally incubated with culture medium before adding the cells. For assays on fluorescent matrices, cells were seeded on either fibronectin–TRITC (Cytoskeleton), Col-IV–FITC or Col-I–FITC (Invitrogen), laminin–FITC (a kind gift from Jean-Philippe Bouchara, Groupe d'Etude des Interactions Hôte-Pathogène, Université d'Angers, France), as indicated above and, after adhesion, treated or not with VEGF-A for the time indicated, then fixed and processed for immunofluorescence staining. Quantification of degradation areas on fluorescence-labelled matrices was performed for at least 10 fields (×10 objective lens) for each coverslip. The areas of degradation were quantified by using ImageJ software. Degraded areas were thresholded and measured by the Analyze Particles function of ImageJ software. The loss of matrix-associated fluorescence (total degraded areas) is presented as the intensity of matrix degradation. The total degradation area (expressed in μm^2) was then normalised for the number of cells (degradation index). Control values were arbitrarily taken as 100%.

Biotinylation of cell surface proteins

Cells (on a 6-cm dish) were washed twice with ice-cold PBS and 0.5 mg/ml EZ-Link™ Sulfo-NHS-Biotin (Thermo Scientific) was added for 30 min (under constant shaking at 4°C). Cells were washed twice with quenching solution (100 mM Glycine in PBS) followed by quenching for 15 min (under constant shaking at 4°C). Cells were washed twice with PBS and lysed with 300 µl immunoprecipitation buffer [20 mM Tris-HCl pH 7.6, 150 mM NaCl, 1% Triton X-100, 1 mM EDTA pH 8, 1 mM EGTA pH 8, 2.5 mM pyrophosphate, 1 mM β-glycerophosphate, protease inhibitor cocktail solution added at 1:25 dilution and phosphoSTOP phosphatase inhibitor solution added at 1:10 dilution (Roche)]. Biotin-labelled material was captured by streptavidin–Sepharose beads (GE Healthcare). Biotinylated cell surface fractions and intracellular fractions were separated and analysed by immunoblotting. Bound proteins were detected by western blot analysis.

Cell transfection with plasmids or siRNA

siRNA transfection into HMVECs was performed by transfection with double-stranded short interfering RNA (siRNA, 50 nM) using the Nucleofector technology. The 21-bp duplex Smartpools of siRNA used for p190RhoGAP-A (sc-44077), p190RhoGAP-B (sc-97682), ARAP3 (sc-61988) were obtained from Santa Cruz. Control siRNA (All-star negative control, #1027281) was purchased from Qiagen. Cells were stimulated with VEGF-A 24 h after transfection as indicated above and analysed.

Antibodies

Antibodies against cortactin (clone 4F11), P-tyrosine (clone 4G10, Platinum, #05-1050), fascin, αVβ3 (clone LM609, MAB1976) and integrin α6 (clone GoH3, MAB135) were obtained from Millipore. Antibodies against N-WASp (clone 30D10, #4848) were from Cell Signaling Technologies. Antibodies against pMLC (Ab2480), MT1-MMP (Ab51074), Nck1 (Ab14588), laminins (Ab30320), DynII (Ab3457) and Col-I (Ab6308) were from Abcam. Antibodies against Grb2 (LB-B4079) were from Lifespan

Journal of Cell Science (2016) 129, 2586-2598 doi:10.1242/jcs.186585

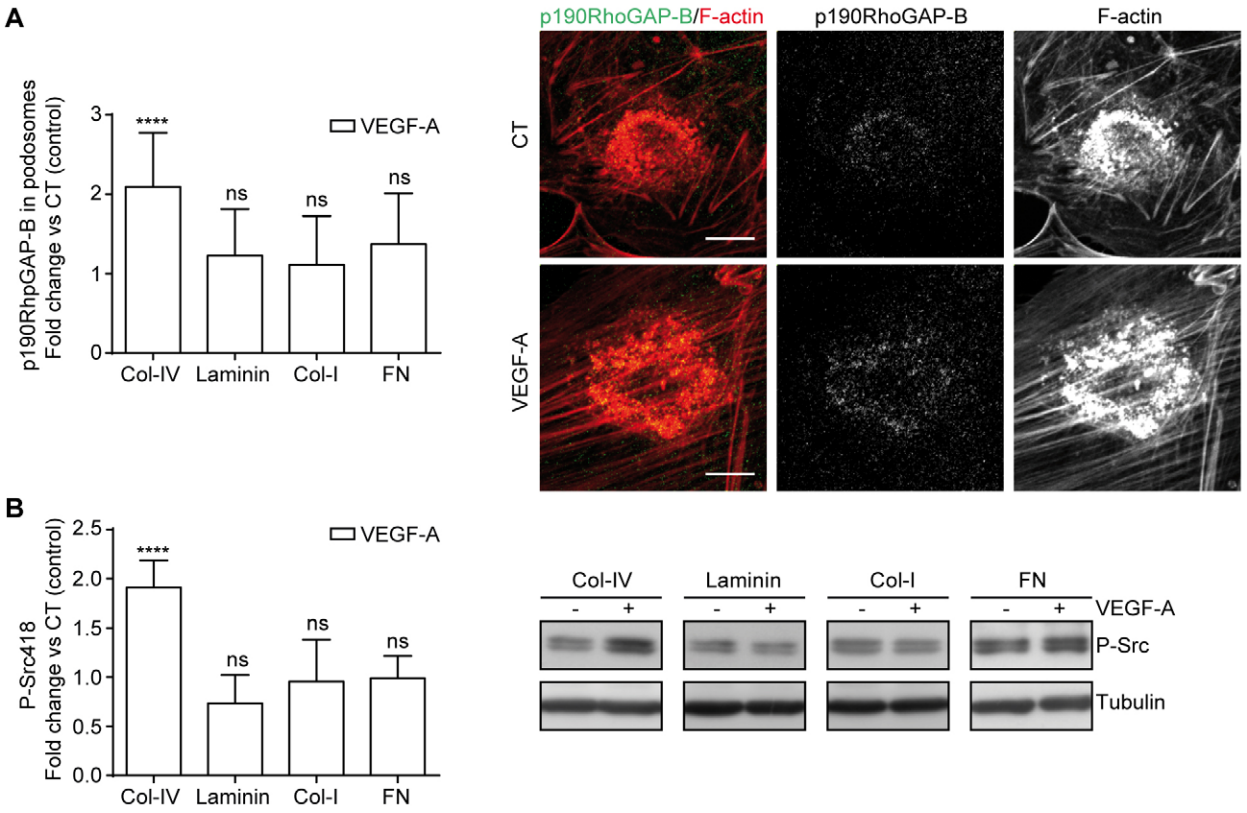

Fig. 6. Matrix-dependent podosome specificities: Col-IV enhances VEGF-A-induced Src autophosphorylation and p190RhoGAP-B recruitment at podosomes. (A) The left panel shows a quantitative analysis of p190RhoGAP-B localisation at podosomes for cells seeded on the indicated substrate presented as integrated density (defined as the product of area and mean grey value) showing increased recruitment of the protein at podosomes in VEGF-A-stimulated cells seeded on Col-IV; *n*=3 independent experiments in which 10 rosettes per experimental point were analysed, mean±s.d. is shown. FN, fibronectin. Fold change compared to the control (CT) in each group is shown. ****P<0.0001; ns, not significant (one-way ANOVA with Bonferroni multiple comparison test). The right panel shows representative images showing differential p190RhoGAP-B staining at podosome rosettes in untreated and VEGF-A-stimulated HMVECs seeded on Col-IV-coated coverslips, counterstained with phalloidin. Scale bars: 10 µm. (B) The left panel shows a quantitative analysis of Src autophosphorylation on Y-418 (P-Src418) in protein extracts from control and VEGF-A-stimulated cells growing on the indicated substrate; the quantification shown in the graph indicates the fold increase in their expression normalised to tubulin in each condition from five independent experiments, mean±s.d. is shown. ****P<0.0001; ns, not significant (one-way ANOVA Bonferroni multiple comparison test compared with the respective CT). The right panel shows a representative image of western blots showing the autophosphorylation on Y-418 (P-Src) in protein extracts from control and VEGF-A-treated (24 h) HMVECs seeded on culture dishes coated with the various matrix proteins.

Biosciences. Antibodies against Tks5 (sc-30122), CD44 (sc-7946), IQGAP (sc-376383) were obtained from Santa Cruz Biotechnology. Antibodies against P-Y418-Src were from MBL (#AT-7135). Antibodies against Fgd1 (#HPA000911), myosin IIA (#M8064), vinculin (clone hVIN-1, #V9131), ARAP3 (#HPA042887), tubulin (clone DM1A, #T9026) and fibronectin (#F3648) were purchased from Sigma. Cleaved Col-I antibodies (targeting the cleavage site, G775-I776) were obtained from ImmunoGlobe®. Antibodies against CD34 (#M-6175) were obtained from Dako. Antibodies against Dbnl were purchased from Proteintech (#13015-1-AP). Monoclonal antibodies against p190RhoGAP-A (#610150) and p190RhoGAP-B (#611613) were obtained from BD Biosciences. Conformation-specific antibodies for RhoA-GTP- were from NewEast Biosciences (#26904). Laboratory-made antibodies against integrin α2 (clone JBS2) were a gift from Linda Pilarski (Cross Cancer Institute, Canada), those against Arp2/3 were kindly given by Matthew Welch (University of California, Berkeley, CA) and those against WIP were kindly given by Ines Anton (CNB-CSIC, Madrid, Spain). For secondary detection, species-specific Alexa-Fluor-488- or Alexa- Fluor-647-labelled secondary antibodies (Jackson Laboratories) were used.

Western blot analysis

Cells were washed in ice-cold PBS and cell lysates were prepared by adding 100 µl of Laemmli buffer on cell monolayers. Samples were boiled for 5 min. Cell lysates (20 µg of proteins) were subjected to SDS-PAGE and proteins were transferred from gels onto immobilon polyvinylidene

Table 1. The responses of microvascular endothelial cells on different matrices upon VEGF-A stimulation

ECM-coating with VEGF-A	None	Gelatin	Matrigel	Col-IV	Laminin	Col-I	FN
Outcome							
Induced podosomes	+	+	+	+	+	–	–
p190RhoGAP-B localisation at podosomes	+	+*	ND	+	–	–	–
Src autophosphorylation	+	+*	ND	+	–	–	–
Matrix degradation	NA	+	ND	+	–	–	–
MT1-MMP cell surface exposure at podosomes	+	+	–	+	–	ND	ND

–, +: no increase and increase, respectively; *data not shown; FN, fibronectin; NA, not applicable; ND, not done.

difluoride membranes (GE Healthcare). Membranes were saturated with 5% bovine serum albumin in Tris-buffered saline containing 0.1% Tween 20 for 1 h and incubated with appropriate primary antibodies (used at a 1:500 dilution except those against tubulin and β-actin that were used at a 1:10,000 dilution). Overnight at 4°C. Then, primary antibodies were revealed using horseradish-peroxidase-coupled anti-mouse-IgG or anti-rabbit-IgG (Jackson laboratories) secondary antibodies for 1 h. Finally, horseradish peroxidase activity was revealed using a chemiluminescence kit (GE-healthcare) according to the manufacturer's instructions. The amounts of proteins detected by western blotting were determined by scanning the autoradiograph (densitometry), followed by processing of the data with ImageJ. All values were normalised against tubulin or β-actin, which was used as a loading control.

Indirect immunofluorescence

Subconfluent cells (unless otherwise indicated) were fixed for 30 min at room temperature in 4% (w/v) paraformaldehyde in PBS and permeabilised with 0.1% Triton X-100 (Sigma) and incubated with primary antibodies (1:100, except cortactin and vinculin, 1:300). F-actin was visualised with Alexa-Fluor-546- or -488-conjugated phalloidin and, when indicated, the nuclei were stained using Hoechst 33342 (Molecular Probes) together with secondary antibodies (1:100). For MT1-MMP cell surface exposure, the permeabilisation step was omitted and cells were incubated for 1 h with MT1-MMP antibodies after several PBS washes. Another 30 min step with 4% PFA was performed to fix the antibodies before permeabilising with 0.1% Triton X-100 and immunofluorescent staining as above. The coverslips were washed in water and mounted on microscope slides with ProLong Gold Antifade containing (or not containing) 4′,6-diamidino-2-phenylindole (DAPI; Life Technologies). For STED, phalloidin-conjugated Alexa-ATTO 647N (Invitrogen) for F-actin detection or ATTO647N-labelled secondary antibodies (Invitrogen) for vinculin or cortactin detection were used (at a 1:100 dilution).

Confocal fluorescence imaging and image analysis

Confocal fluorescent images were acquired with a Zeiss LSM 510 Meta inverted laser scanning fluorescence microscope equipped with acquisition software (LSM 510 acquisition software; Zeiss) and a ×63 NA 1.4 oil immersion objective. Triple- or quadruple-colour imaging for DAPI or Hoechst 33342, Alexa-Fluor-546–phalloidin, and Alexa-Fluor-488-labelled and/or Alexa-Fluor-647-labelled secondary antibodies was performed using selective laser excitation at 350, 543, 488 and/or 647 nm, respectively. Each channel was imaged sequentially using the multitrack recording module before merging. Cells showing podosome rosettes were quantified by scoring at least 300 cells for each coverslip. Quantification of proteins at podosome rosettes was computed using the ImageJ Analyze Particles function by taking the mask of the rosette according to the cortactin staining and applying the mask to the image corresponding to the protein analysed. Integrated density was used as readout. To analyse the number of podosomes presenting MTI-MMP, F-actin- and cortactin-positive podosome dots were scored when positive for MT1-MMP. STED super-resolution images were acquired with a Leica DMI6000 inverted TCS SP5 AOBS microscope combined with the regular confocal mode for the companion markers.

Time-lapse microscopy

To assess cell motility, HMVECs were seeded at a density of 15×10^3cells per well on Oregon-Green-488–gelatin-coated glass-bottom 24-well plates (Greiner). Hoescht 33342 (10 ng/ml) was added to label the nuclei and the cells were either left untreated or treated with 25 ng/ml of VEGF-A. Live-cell imaging was performed with a Eclipe Ti Nikon videomicroscope coupled with NIS analysis software, based on a 10× NA 0.30 objective lens (Nikon), a Hamamatsu Digital CCD C10600-10B camera, and an environmental chamber to maintain cells at 37°C in a 5% CO_2 humidified atmosphere (Life Imaging Services). Videos were acquired every 15 min for a period of 3 h in bright-field, green and blue filters (Oregon-Green-488–gelatin and Hoescht 33342, respectively). Mean cell velocity and cell displacement were calculated with the ImageJ plugin TrackMate. The software was used to automatically track nuclei and characterise their trajectories amongst stacks of images.

Statistics

Each experiment was performed at least three times and quantification values represent the mean±s.d. of three independent experiments if not stated otherwise. Statistical analysis was performed with GraphPad Prism 6 (GraphPad Software, Inc., San Diego, CA). Significance was determined by using a Student's *t*-test or one-way ANOVA (Bonferroni multiple comparison test between selected pairs), and $P<0.05$ was considered statistically significant.

Acknowledgements

We thank Prof. Andreas Bikfalvi for sharing some of the reagents used in the study and Laure-Anne Cussac for help with quantification experiments. We thank Dr J. P. Bouchara (Groupe d'Etude des Interactions Hôte-Pathogène, EA 3142, Université d'Angers, France) for providing laminin–FITC, Dr Linda Pilarski (University of Alberta, Canada) for providing anti-integrin-α2 antibodies (JBS2) and Ines Antón (CNB-CSIC), Madrid, Spain) for providing WIP antibodies. We also thank Ray Cooke for editing of the manuscript prior to submission.

Competing interests

The authors declare no competing or financial interests.

Author contributions

T.D., P.S. and E.G. designed the biological experiments. T.D., P.S., I.F., F.A. and E.G. performed the experiments. P.S. and E.G. wrote the manuscript. All authors discussed the results and commented on the manuscript.

Funding

This work was supported by Institut National de la Santé et de la Recherche Médicale (INSERM); the Ligue Contre le Cancer (Comité des Pyrénées Atlantiques); and the Fondation de France [grant number 00056836]. P. S. was supported by a grant from Ligue Contre le Cancer; and T.D. by a fellowship from Association pour la Recherche sur le Cancer. F.A. received financial support from the French State in the framework of the 'Investments for the future' Program IdEx Bordeaux [grant number ANR #-10-IDEX-03-02].

Supplementary information

Supplementary information available online at
http://jcs.biologists.org/lookup/doi/10.1242/jcs.186585.supplemental

References

Billottet, C., Rottiers, P., Tatin, F., Varon, C., Reuzeau, E., Maitre, J. L., Saltel, F., Moreau, V. and Genot, E. (2008). Regulatory signals for endothelial podosome formation. *Eur. J. Cell Biol.* **87**, 543-554.

Caron, C., Spring, K., Laramée, M., Chabot, C., Cloutier, M., Gu, H. and Royal, I. (2009). Non-redundant roles of the Gab1 and Gab2 scaffolding adapters in VEGF-mediated signalling, migration, and survival of endothelial cells. *Cell. Signal.* **21**, 943-953.

Chun, T.-H., Sabeh, F., Ota, I., Murphy, H., McDonagh, K. T., Holmbeck, K., Birkedal-Hansen, H., Allen, E. D. and Weiss, S. J. (2004). MT1-MMP-dependent neovessel formation within the confines of the three-dimensional extracellular matrix. *J. Cell Biol.* **167**, 757-767.

Claesson-Welsh, L. and Welsh, M. (2013). VEGFA and tumour angiogenesis. *J. Intern. Med.* **273**, 114-127.

Curado, F., Spuul, P., Egana, I., Rottiers, P., Daubon, T., Veillat, V., Duhamel, P., Leclercq, A., Gontier, E. and Génot, E. (2014). ALK5 and ALK1 play antagonistic roles in TGFbeta-induced podosome formation in aortic endothelial cells. *Mol. Cell. Biol.* **34**, 4389-4403.

Davis, G. E. and Senger, D. R. (2005). Endothelial extracellular matrix: biosynthesis, remodeling, and functions during vascular morphogenesis and neovessel stabilization. *Circ. Res.* **97**, 1093-1107.

Fuller, K., Ross, J. L., Szewczyk, K. A., Moss, R. and Chambers, T. J. (2010). Bone is not essential for osteoclast activation. *PLoS ONE* **5**, e12837.

Guegan, F., Tatin, F., Leste-Lasserre, T., Drutel, G., Genot, E. and Moreau, V. (2008). p190B RhoGAP regulates endothelial-cell-associated proteolysis through MT1-MMP and MMP2. *J. Cell Sci.* **121**, 2054-2061.

Juin, A., Billottet, C., Moreau, V., Destaing, O., Albiges-Rizo, C., Rosenbaum, J., Genot, E. and Saltel, F. (2012). Physiological type I collagen organization induces the formation of a novel class of linear invadosomes. *Mol. Biol. Cell* **23**, 297-309.

Juin, A., Planus, E., Guillemot, F., Horakova, P., Albiges-Rizo, C., Génot, E., Rosenbaum, J., Moreau, V. and Saltel, F. (2013). Extracellular matrix rigidity

controls podosome induction in microvascular endothelial cells. *Biol. Cell* **105**, 46-57.

Kremerskothen, J., Stolting, M., Wiesner, C., Korb-Pap, A., van Vliet, V., Linder, S., Huber, T. B., Rottiers, P., Reuzeau, E., Genot, E. et al. (2010). Zona occludens proteins modulate podosome formation and function. *FASEB J.* **25**, 505-514.

Labernadie, A., Thibault, C., Vieu, C., Maridonneau-Parini, I. and Charriere, G. M. (2010). Dynamics of podosome stiffness revealed by atomic force microscopy. *Proc. Natl. Acad. Sci. USA* **107**, 21016-21021.

Le Bail, B., Bioulac-Sage, P., Senuita, R., Quinton, A., Saric, J. and Balabaud, C. (1990). Fine structure of hepatic sinusoids and sinusoidal cells in disease. *J. Electron Microsc. Tech.* **14**, 257-282.

Linder, S. (2007). The matrix corroded: podosomes and invadopodia in extracellular matrix degradation. *Trends Cell Biol.* **17**, 107-117.

Linder, S. and Aepfelbacher, M. (2003). Podosomes: adhesion hot-spots of invasive cells. *Trends Cell Biol.* **13**, 376-385.

Linder, S. and Kopp, P. (2005). Podosomes at a glance. *J. Cell Sci.* **118**, 2079-2082.

Linder, S. and Wiesner, C. (2015). Tools of the trade: podosomes as multipurpose organelles of monocytic cells. *Cell. Mol. Life Sci.* **72**, 121-135.

Luxenburg, C., Geblinger, D., Klein, E., Anderson, K., Hanein, D., Geiger, B. and Addadi, L. (2007). The architecture of the adhesive apparatus of cultured osteoclasts: from podosome formation to sealing zone assembly. *PLoS ONE* **2**, e179.

Matheson, S. F., Hu, K.-Q., Brouns, M. R., Sordella, R., VanderHeide, J. D. and Settleman, J. (2006). Distinct but overlapping functions for the closely related p190 RhoGAPs in neural development. *Dev. Neurosci.* **28**, 538-550.

Meyer, R. D., Sacks, D. B. and Rahimi, N. (2008). IQGAP1-dependent signaling pathway regulates endothelial cell proliferation and angiogenesis. *PLoS ONE* **3**, e3848.

Murphy, D. A. and Courtneidge, S. A. (2011). The 'ins' and 'outs' of podosomes and invadopodia: characteristics, formation and function. *Nat. Rev. Mol. Cell Biol.* **12**, 413-426.

Norrby, K. (2006). In vivo models of angiogenesis. *J. Cell. Mol. Med.* **10**, 588-612.

Osiak, A.-E., Zenner, G. and Linder, S. (2005). Subconfluent endothelial cells form podosomes downstream of cytokine and RhoGTPase signaling. *Exp. Cell Res.* **307**, 342-353.

Phng, L.-K. and Gerhardt, H. (2009). Angiogenesis: a team effort coordinated by notch. *Dev. Cell* **16**, 196-208.

Plow, E. F., Meller, J. and Byzova, T. V. (2014). Integrin function in vascular biology: a view from 2013. *Curr. Opin Hematol.* **21**, 241-247.

Ponik, S. M., Trier, S. M., Wozniak, M. A., Eliceiri, K. W. and Keely, P. J. (2013). RhoA is down-regulated at cell-cell contacts via p190RhoGAP-B in response to tensional homeostasis. *Mol. Biol. Cell* **24**, 1688-1699, S1-S3.

Proag, A., Bouissou, A., Mangeat, T., Voituriez, R., Delobelle, P., Thibault, C., Vieu, C., Maridonneau-Parini, I. and Poincloux, R. (2015). Working together: spatial synchrony in the force and actin dynamics of podosome first neighbors. *ACS Nano* **9**, 3800-3813.

Rottiers, P., Saltel, F., Daubon, T., Chaigne-Delalande, B., Tridon, V., Billottet, C., Reuzeau, E. and Genot, E. (2009). TGFbeta-induced endothelial podosomes mediate basement membrane collagen degradation in arterial vessels. *J. Cell Sci.* **122**, 4311-4318.

Rowe, R. G. and Weiss, S. J. (2008). Breaching the basement membrane: who, when and how? *Trends Cell Biol.* **18**, 560-574.

Seano, G., Chiaverina, G., Gagliardi, P. A., di Blasio, L., Puliafito, A., Bouvard, C., Sessa, R., Tarone, G., Sorokin, L., Helley, D. et al. (2014). Endothelial podosome rosettes regulate vascular branching in tumour angiogenesis. *Nat. Cell Biol.* **16**, 931-941.

Siemerink, M. J., Klaassen, I., Vogels, I. M., Griffioen, A. W., Van Noorden, C. J. and Schlingemann, R. O. (2012). CD34 marks angiogenic tip cells in human vascular endothelial cell cultures. *Angiogenesis* **15**, 151-163.

Spuul, P., Chi, P.-Y., Billottet, C., Chou, C.-F. and Génot, E. (2015). Microfluidic devices for the study of actin cytoskeleton in constricted environments: evidence for podosome formation in endothelial cells exposed to a confined slit. *Methods.* **94**, 65-74.

Sun, Z., Li, X., Massena, S., Kutschera, S., Padhan, N., Gualandi, L., Sundvold-Gjerstad, V., Gustafsson, K., Choy, W. W., Zang, G. et al. (2012). VEGFR2 induces c-Src signaling and vascular permeability in vivo via the adaptor protein TSAd. *J. Exp. Med.* **209**, 1363-1377.

Tatin, F., Varon, C., Génot, E. and Moreau, V. (2006). A signalling cascade involving PKC, Src and Cdc42 regulates podosome assembly in cultured endothelial cells in response to phorbol ester. *J. Cell Sci.* **119**, 769-781.

van den Dries, K., Meddens, M. B., de Keijzer, S., Shekhar, S., Subramaniam, V., Figdor, C. G. and Cambi, A. (2013). Interplay between myosin IIA-mediated contractility and actin network integrity orchestrates podosome composition and oscillations. *Nat. Commun.* **4**, 1412.

Varon, C., Tatin, F., Moreau, V., Van Obberghen-Schilling, E., Fernandez-Sauze, S., Reuzeau, E., Kramer, I. and Genot, E. (2006). Transforming growth factor beta induces rosettes of podosomes in primary aortic endothelial cells. *Mol. Cell. Biol.* **26**, 3582-3594.

Veillat, V., Spuul, P., Daubon, T., Egaña, I., Kramer, I. and Génot, E. (2015). Podosomes: multipurpose organelles? *Int. J. Biochem. Cell Biol.* **65**, 52-60.

Walde, M., Monypenny, J., Heintzmann, R., Jones, G. E. and Cox, S. (2014). Vinculin binding angle in podosomes revealed by high resolution microscopy. *PLoS One* **9**, e88251.

Wiesner, C., Faix, J., Himmel, M., Bentzien, F. and Linder, S. (2010). KIF5B and KIF3A/KIF3B kinesins drive MT1-MMP surface exposure, CD44 shedding, and extracellular matrix degradation in primary macrophages. *Blood* **116**, 1559-1569.

Yu, C.-H., Rafiq, N. B. M., Krishnasamy, A., Hartman, K. L., Jones, G. E., Bershadsky, A. D. and Sheetz, M. P. (2013). Integrin-matrix clusters form podosome-like adhesions in the absence of traction forces. *Cell Rep.* **5**, 1456-1468.

Yurchenco, P. D., Amenta, P. S. and Patton, B. L. (2004). Basement membrane assembly, stability and activities observed through a developmental lens. *Matrix. Biol.* **22**, 521-538.

Journal of Cell Science